J. MATER. CHEM., 1995, 5(7), 1075–1080

Mechanisms for the Thermal Decomposition of NH_4VO_3 into V_6O_{13}, V_3O_7 and V_2O_5

Christina Lampe-Önnerud and John O. Thomas*
Institute of Chemistry, Uppsala University, Box 531, S-751 21 Uppsala, Sweden

The thermal decomposition of ammonium metavanadate, NH_4VO_3, has been studied by differential scanning calorimetry (DSC), mass spectrometry (MS) and X-ray diffraction (XRD) in the temperature range 50–500 °C. Different experimental conditions (heating rate and atmosphere) have been explored in various combinations. Different types of reaction mechanisms leading to crystalline V_6O_{13} and V_3O_7 can be identified. The formation of V_2O_5 is also discussed briefly.

Thin-film lithium-polymer batteries, incorporating some vanadium oxide phase as cathode material, have attracted considerable interest in recent years. Vanadium oxides with compositions close to that of V_6O_{13} are of particular interest as intercalation hosts. However, it has been difficult to obtain consistently phase-pure V_6O_{13}; other vanadium oxides such as V_2O_5, V_3O_7 and VO_2 are frequently found as impurity phases.[1] The most common way to prepare vanadium oxides is *via* the thermal decomposition of ammonium metavanadate, NH_4VO_3, recovered from the hydrometallurgical treatment of vanadium ores. Several authors have studied this decomposition, but the literature gives an inconsistent picture. The most commonly studied form of vanadium oxide is V_2O_5,[2–8] but the proposed reaction mechanisms involved differ greatly. Some claim (*e.g.* ref. 5) that ammonium metavanadate is converted endothermically in vacuum, air and argon atmospheres first to ammonium bivanadate, and then to ammonium hexavanadate, before V_2O_5 is formed. Askar *et al.*[8] agree on an endothermic process, but claim that the decomposition occurs in only two steps. Others have identified intermediates lacking ammonium; these were shown to be endothermically formed hydrates of vanadium oxides: $V_2O_5 \cdot H_2O$[7] or $V_3O_7 \cdot H_2O$.[2] An exothermal reaction then follows to give V_2O_5, which it is claimed transforms into V_3O_7, V_6O_{13} and VO_2. Von Sacken and Dahn[9] have studied the formation of V_2O_5 and how excess NH_3 facilitates the formation of V_2O_3. They also report difficulties in achieving a controlled formation of several VO_x compounds in a homogeneous powder form.

In this work, the experimental conditions for the thermal decomposition of NH_4VO_3 have been studied for some of the more commonly occurring vanadium oxides (V_2O_5, V_3O_7 and V_6O_{13}). Studies of the conditions for the formation of the lower vanadium oxide, VO_2, are in progress.

Experimental

The starting material for all experiments was NH_4VO_3 powder (Gesellschaft für Elektrometallurgie, MBH, 99.9%). No pre-treatment was performed. The thermal decomposition experiments were carried out using a differential scanning calorimeter of type Mettler TA 4000 in a flushing nitrogen atmosphere with an aluminium reference. Prior to the experiments, calibrations with a standard sample of Ln, Pb and Zn at two different heating rates (1 and 10 °C min^{-1}) were performed. The temperature range used was 50–500 °C, but samples were taken at several intermediate temperatures and quenched to room temperature (< 20 s) with cooled nitrogen gas to study the mechanism. In order to probe the effect of heating rate on the mechanism of decomposition, the scanning rate was varied between 0.5 and 40 °C min^{-1}. In all experiments, 14 mg of the NH_4VO_3 powder was placed in an aluminium crucible (< 0.2 cm^3). The number of reproducibly standard holes in the crucible lid (10, 1, 0) was varied to assess the effect of the initially formed gaseous products on the subsequent reaction steps.

The presence of gaseous species formed during the thermal decomposition was studied in a specially designed system. The sample, placed in a quartz tube, was heated as for the DSC experiments. Helium was used as carrier gas to lead the species formed to a mass spectrometer equipped with a quadrupole detector (Balzers QMG 420).

The nitrogen content in the final products was determined by the Kjeldahl method,[10] whereby all nitrogen in the sample is first converted to ammonium ions, which are then treated with an excess of some strong base to form ammonia and water. The ammonia liberated is then carefully titrated.

As a control experiment for the mechanisms presented below, V_2O_5 was prepared by heating NHY_4VO_3 for 12 h at 500 °C in air.

All samples were characterized in terms of their phase and degree of crystallinity by XRD with Cu-Kα_1 radiation using a STOE & CIE GmbH STADI powder diffractometer fitted with a curved, position-sensitive detector. The stabilities of intermediate phases formed along the reaction path were assessed. The standard procedure for the diffraction experiments was a short (2 min) exposure followed by a longer (30 min) exposure.

Results

The different experimental conditions give three different DSC curves. The *first* [Fig. 1(*a*)] is obtained using a heating rate of 10 °C min^{-1} and one hole in the crucible lid. The three peaks, A1, B and C, seen in the DSC measurements, correspond to the formation of $V_3O_7 \cdot H_2O$,[11] some amorphous phase and V_3O_7 [12] observed with XRD [Fig. 2(*a*), (*c*) and Fig. 3]. The diffractograms shown in Fig. 2 are taken for samples quenched at their corresponding DSC peak maxima. This somewhat unusual procedure is due to the rapid decomposition that follows the phase transformations. The MS measurements [Fig. 4(*a*)] show that, at both A1 and B, large quantities of NH_3 and H_2O are liberated. No NH_3, but some N_2 closely followed by H_2O can be observed at C. The O_2-sensitivity was high, but none was detected during any of the reaction steps. The processes are almost identical for experiments performed at 20 and 40 °C min^{-1}, although observed enthalpies and temperatures show some variation [Table 1(*a*)]. The phases present are the same as in the standard experiment, but the formation of a mixture of *ca.* 95% V_3O_7–5% V_6O_{13} [13] can be identified for a heating

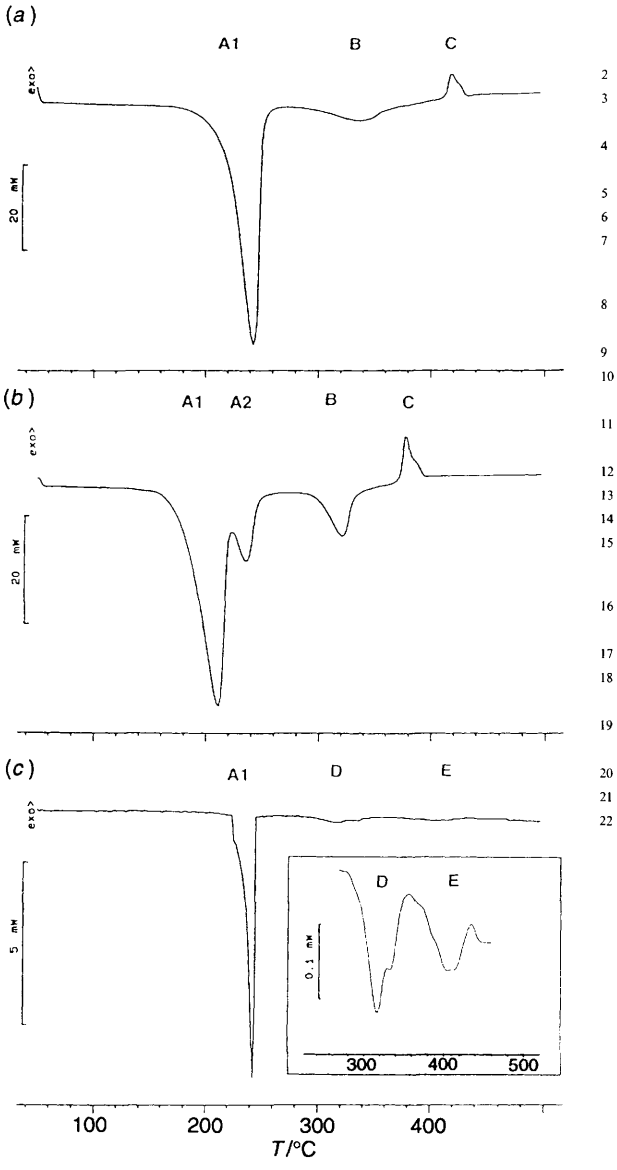

Fig. 1 DSC curves for the decompositon of NH_4VO_3 obtained at: (*a*) 10 °C min^{-1} with 1 hole in the crucible lid (mechanism 1); (*b*) 10 °C min^{-1} and 10 holes in the crucible lid (mechanism 2); and (*c*) 0.5 °C min^{-1} and sealed crucible lid (mechanism 3)

rate of 20 °C min^{-1}, and *ca.* 50% V_3O_7–50% V_6O_{13} for 40 °C min^{-1} at C.

The second type of DSC curve [Fig. 1(*b*)] is obtained for a heating rate of 10 °C min^{-1} both with no lid and with 10 holes in the lid, and at 0.7 °C min^{-1} with one hole in the lid. The phases formed at the different stages are: $V_3O_7 \cdot H_2O$ [reaction step A1; Fig. 2(*a*)], $NH_4V_3O_8 \cdot 1/2H_2O$[14] [reaction step A2; Fig. 2(*b*)], amorphous [reaction step B; Fig. 2(*c*)] and single-phase V_3O_7 (reaction step C; Fig. 3); *ca.* 50% V_2O_5–50% V_3O_7 [15] is also formed with no lid [see Table 1(*b*)]. The mass spectrum [Fig. 4(*b*)] resembles closely that for mechanism 1, with the exception of the new A2 peak. Note the almost equal quantities of NH_3 and H_2O leaving at A1 and A2.

A very different DSC curve [Fig. 1(*c*)] is obtained when heating at 0.5 °C min^{-1} in a sealed aluminium crucible (no hole in lid). The largest peak (A1) corresponds, as in mechanisms 1 and 2, to the formation of $V_3O_7 \cdot H_2O$. However, a fast transformation into an amorphous phase follows, and the crystalline peaks in the XRD measurements disappear in a different order. The mass spectrum [Fig. 4(*c*)] reveals another difference; not only NH_3 and H_2O, but also N_2 is formed towards the end of this first reaction step.

The DSC curve then levels out, showing only two small endothermic processes [see inset in Fig. 1(*c*)]. The X-ray diffractograms show first a complicated atomic rearrangement *via* an amorphous phase (D) into the final single-phase crystalline V_6O_{13} (E) (Fig. 5). When the heating rate is increased, the parallel formation of V_2O_5 starting at (D) can be seen with XRD. Correspondingly, the DSC curves give greater enthalpies, especially at reaction step D [Table 1(*c*)]. In all experiments following mechanism 3, gas overpressure causes a small hole to be formed in the aluminium crucible seal on passing through the A1 peak. The noise in the mass spectrum, showing the release of N_2 and O_2 before reaching the temperature of the A1 peak maximum, can be ascribed to this cracking process. (Further studies with a closed container are published elsewhere.[16])

It was concluded from the Kjeldahl analysis that none of the final products contained nitrogen. It was also confirmed by XRD that the control experiment led to the formation of single-phase V_2O_5 (Fig. 6). The NH_4VO_3 powder was analysed at regular intervals, and shown to be stable and of single phase throughout the study.

Note that the temperatures quoted in Table 1 relate to the peak maximum for each reaction step (with an error of ±0.5°). However, the calculated ΔH values obtained in this study can vary by as much as 20%, especially for the smaller peaks, owing to the problem of defining the background. These values should therefore be used only as a guide in understanding the complicated chemistry involved here.

Table 1 Results from DSC experiments

(*a*) Mechanism 1

DSC peak	10 °C min^{-1}, one hole in lid		20 °C min^{-1}, one hole in lid		40 °C min^{-1}, one hole in lid	
	T/°C	ΔH/J g^{-1}	T/°C	ΔH/J g^{-1}	T/°C	ΔH/J g^{-1}
A1	235	540	239	532	256	481
B	338	60	339	52	354	45
C	414	30	418	30	432	26

(*b*) Mechanism 2

DSC peak	0.7 °C min^{-1}, one hole in lid		10 °C min^{-1}, no lid		10 °C min^{-1}, 10 holes in lid	
	T/°C	ΔH/J g^{-1}	T/°C	ΔH/J g^{-1}	T/°C	ΔH/J g^{-1}
A1	185	362	198	372	207	324
A2	200	33	234	77	235	38
B	298	158	311	105	321	80
C	355	31	374	30	379	42

(*c*) Mechanism 3

DSC peak	0.5 °C min^{-1}, no holes in lid		1 °C min^{-1}, no holes in lid		10 °C min^{-1}, no holes in lid	
	T/°C	ΔH/J g^{-1}	T/°C	ΔH/J g^{-1}	T/°C	ΔH/J g^{-1}
A1	242	543	245	553	269	491
D	315	49	325	60	351	78
E	404	25	415	12	444	27

Discussion

When forming any VO_x species with a mean oxidation number below +5 from NH_4VO_3, two different processes takes place.

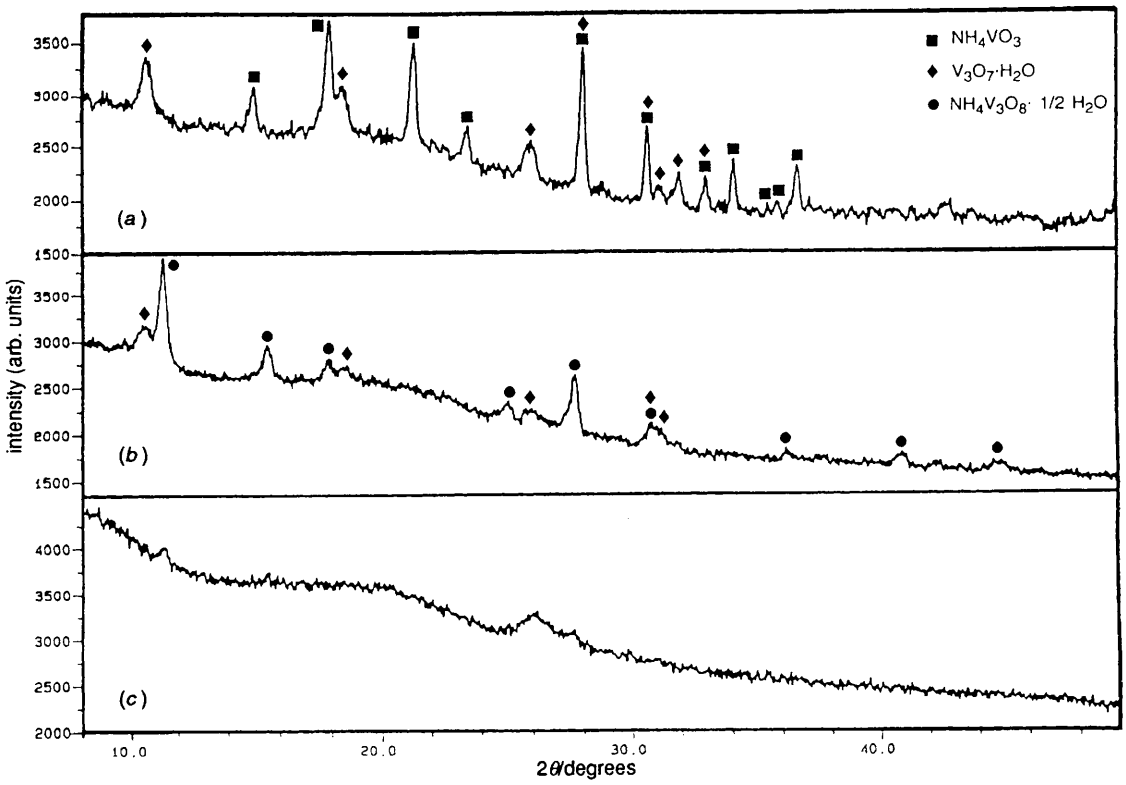

Fig. 2 X-Ray diffractograms for the thermal decomposition of NH_4VO_3 into V_3O_7: (*a*) the first reaction step (A1) in mechanism 1, mechanism 2 and mechanism 3, corresponding to the formation of $V_3O_7 \cdot H_2O$ from NH_4VO_3; (*b*) the coexistence of $V_3O_7 \cdot H_2O$ and $NH_4V_3O_8 \cdot \frac{1}{2}H_2O$ for mechanism 2 only (A2); and (*c*) an amorphous phase appearing for mechanisms 1 and 2 at B

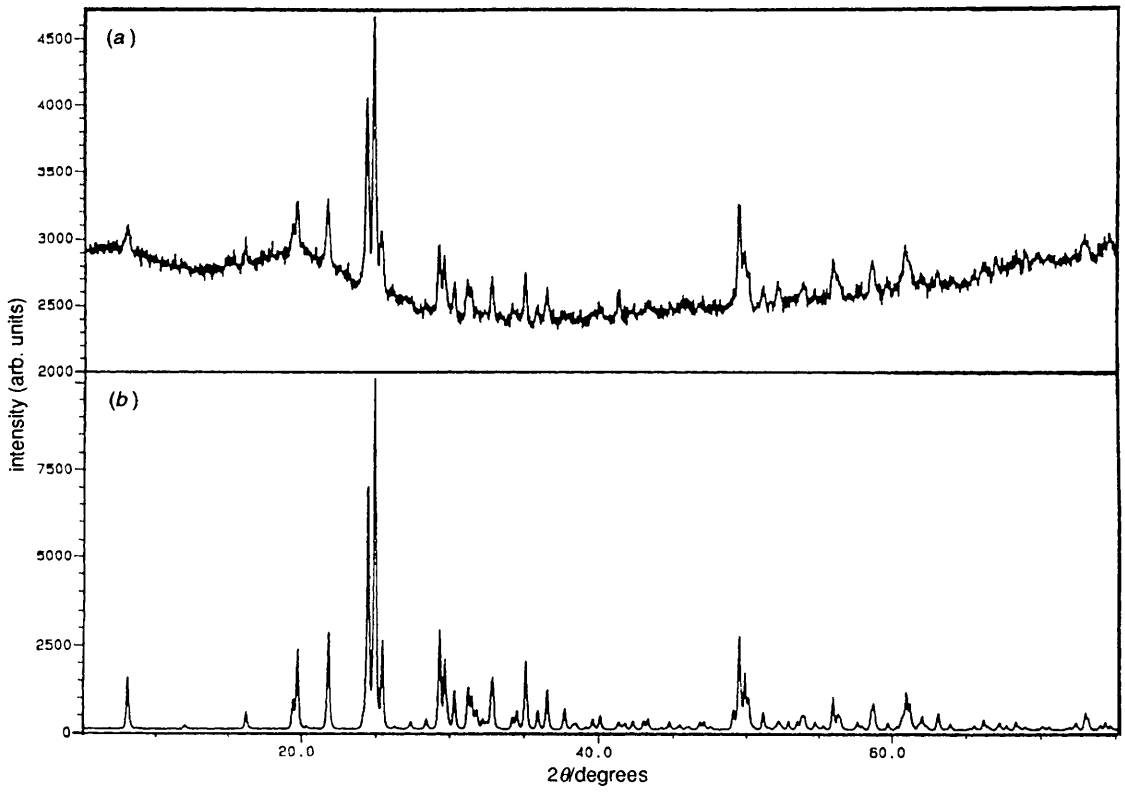

Fig. 3 (*a*) X-Ray diffractogram for the single-phase final product V_3O_7 and (*b*) corresponding calculated X-ray diffractogram (Cu-Kα_1 radiation)

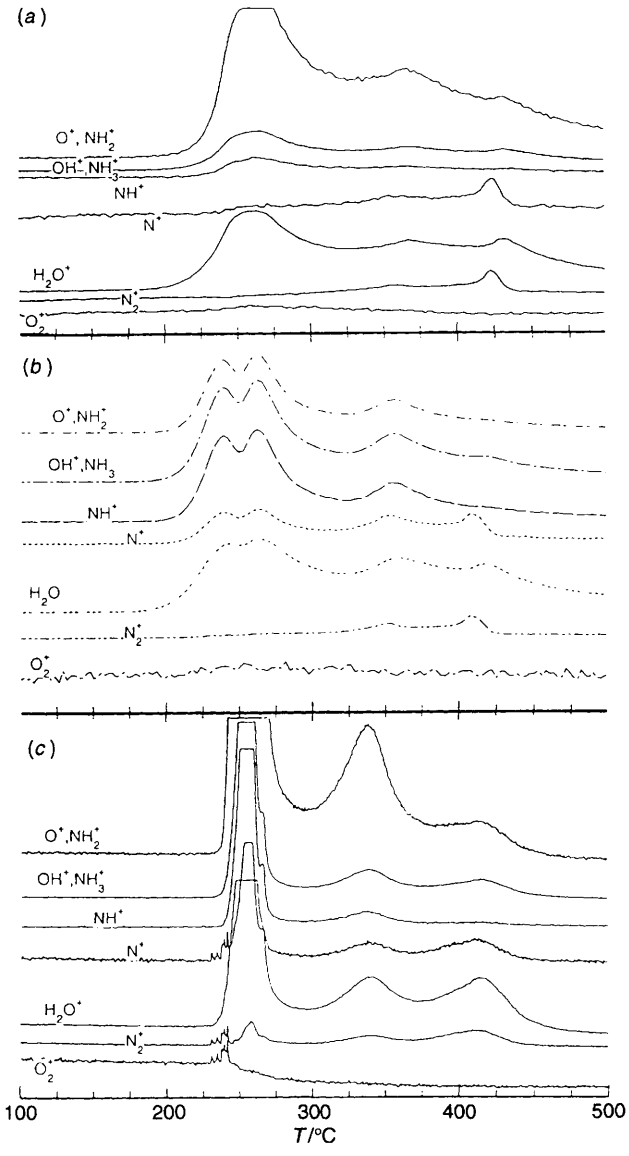

Fig. 4 Mass spectra for the decomposition of NH_4VO_3 obtained at: (*a*) 10 °C min^{-1} with one aluminium crucible (14 mg NH_4VO_3) and one hole in the lid (mechanism 1); (*b*) 10 °C min^{-1} with an open Al_2O_3 crucible (100 mg NH_4VO_3) (mechanism 2); and (*c*) 0.5 °C min^{-1} with 10 sealed aluminium crucibles (10 × 14 mg NH_4VO_3) (mechanism 1)

The first involves the decomposition of NH_4VO_3 into vanadium(+5) oxides with or without an ammonium content. The second can be described as a redox reaction, as the formation of lower oxidation states on the vanadium proceed. These processes can operate simultaneously.

Mechanism 1

The DSC results (Fig. 1) clearly show three different reaction paths. At a heating rate of 10 °C min^{-1}, using one hole in the crucible lid, the DSC curve exhibits three peaks [Fig. 1(*a*)]. The first reaction step (A1) is strongly endothermic and XRD reveals the formation of $V_3O_7 \cdot H_2O$. The mass spectra show that large quantities of NH_3 and H_2O leave the system. The small amount of N_2 formed suggests that vanadium is reduced according to:

$$9NH_4VO_3 \rightarrow 3V_3O_7 \cdot H_2O + 8NH_3 + 3H_2O + \tfrac{1}{2}N_2 \quad (1)$$

This decomposition is followed by a colour change from white NH_4VO_3 *via* dark yellow, for the mixture of the two phases, to reddish brown $V_3O_7 \cdot H_2O$ [reaction step A1, Fig. 2(*a*)]. At the second reaction step (B), which is also endothermic, the intermediate state becomes disordered and an amorphous dark-brown transition state forms [Fig. 2(*c*)]. Peak B corresponds to a decomposition, which will be treated in the following as a single reaction step. The detection of all nitrogen-containing species also suggests that a reduction process occurs in the amorphous phase. The decomposition and atomic rearrangement is also accompanied by NH_3 and H_2O leaving the system. During the third and final reaction step (C), fine structure can be seen in the DSC curve. The first part possibly corresponds to the final reduction of vanadium from mean oxidation number +5 to $+4\frac{2}{3}$ and is exothermic. The second part describes the loss of water of crystallization to form black V_3O_7:

$$V_3O_7 \cdot H_2O \rightarrow V_3O_7 + H_2O \quad (2)$$

On increasing the heating rate to 20 °C min^{-1}, the DSC curve shows the same features. Similar behaviour has also been observed for the decomposition into V_2O_5.[8] XRD also reveals that the final product is no longer the single-phase V_3O_7 formed exothermically according to reaction (2) above. Instead, the final product is a mixture of V_3O_7 (95%) and V_6O_{13} (5%). The formation of V_6O_{13} is endothermic, involving a redox reaction, since the vanadium must go from mean oxidation state +5 to $+4\frac{1}{3}$. The reduction of vanadium is coupled to the oxidation of gaseous products formed during the decomposition. Thus, when the temperature is raised quickly, the gases create an overpressure, which will enhance the reduction of vanadium and the formation of lower oxides.

This trend is even more pronounced when the heating rate is increased to 40 °C min^{-1}. Here, the three reaction steps are shifted to even higher temperatures, and the fraction of V_6O_{13} formed increases to about 50%.

As can be seen in Table 1, not only the temperatures but also the observed ΔH values are influenced by the heating rate; the first reaction step has the greatest ΔH. XRD shows a lower peak-to-background ratio for the V_3O_7 peaks at the higher heating rate, *i.e.* 0.4 and 0.8 for 40 and 10 °C min^{-1}, respectively. This is due partly to the formation of V_6O_{13}, and partly to the decrease in particle size (seen as peak broadening in XRD).

Mechanism 2

A different route is followed on increasing the number of holes to 10 in the crucible lid, and keeping the heating rate at 10 °C min^{-1}. The DSC curve [Fig. 1(*b*)] now exhibits four peaks for the decomposition of NH_4VO_3. As in the case of mechanism 1, the first reaction step (A1) is the most energetic, with XRD [Fig. 2(*a*)] indicating the formation of $V_3O_7 \cdot H_2O$ according to reaction (1) above. The next reaction step (A2) is closely related to A1, with gaseous ammonia, nitrogen and water being evolved continuously. Since the gases can here diffuse out more easily from the crucible, reaction (1) is shifted to the right. XRD shows that $V_3O_7 \cdot H_2O$ still exists at A2. However, no NH_4VO_3 is present; instead a new phase, $NH_4V_3O_8 \cdot \frac{1}{2}H_2O$, has been formed [Fig. 2(*b*)]:

$$3NH_4VO_3 \rightarrow NH_4V_3O_8 \cdot \tfrac{1}{2}H_2O + 2NH_3 + \tfrac{1}{2}H_2O \quad (3)$$

Vanadium here retains oxidation state +5 and a decomposition process occurs. The redox reaction to convert the whole sample to $V_3O_7 \cdot H_2O$ then follows:

$$6NH_4V_3O_8 \cdot \tfrac{1}{2}H_2O \rightarrow 6V_3O_7 \cdot H_2O + 4NH_3 + 3H_2O + N_2 \quad (4)$$

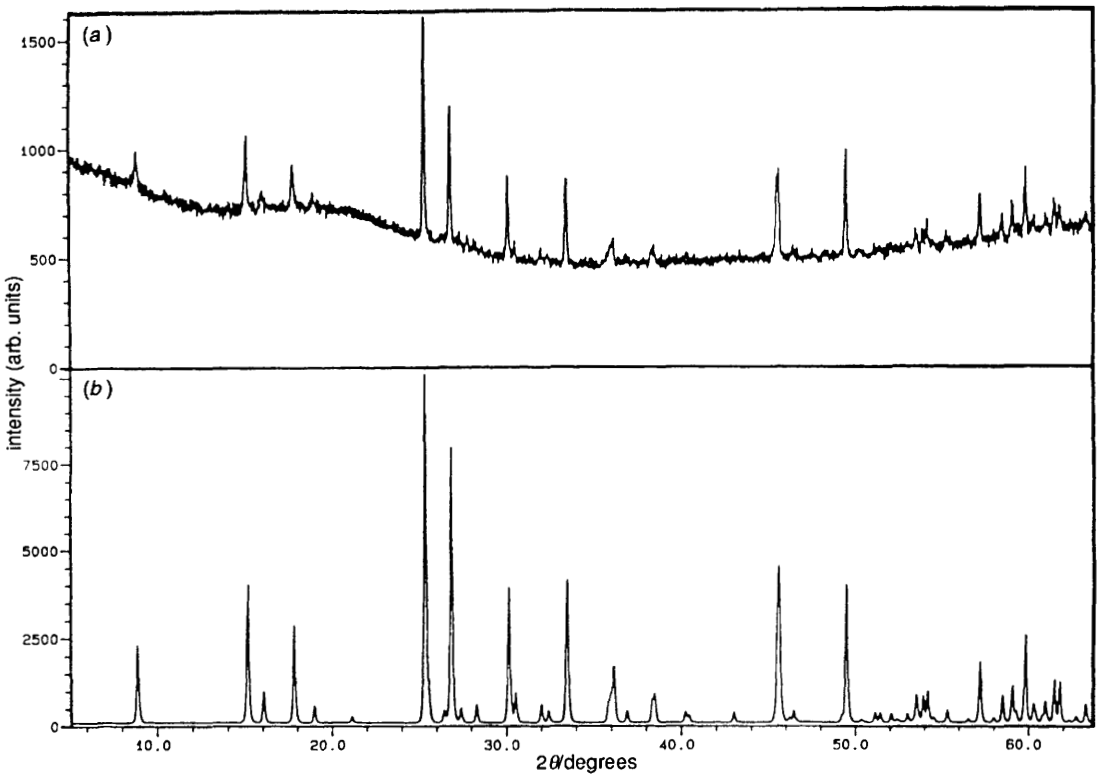

Fig. 5 (*a*) X-Ray diffractogram for the single-phase final product V_6O_{13}; and (*b*) corresponding calculated X-ray diffractogram (Cu-Kα_1 radiation)

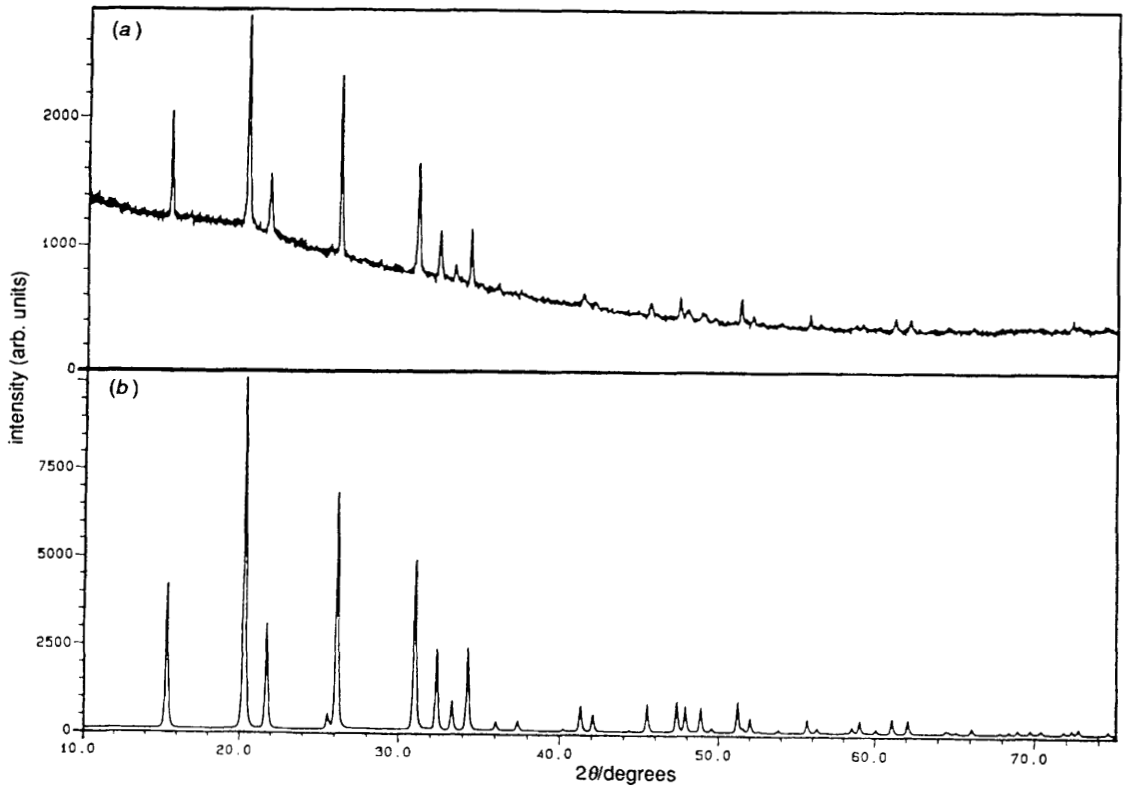

Fig. 6 (*a*) X-Ray diffractogram for the single-phase V_2O_5 formed in the control experiment; and (*b*) corresponding calculated X-ray diffractogram (Cu-Kα_1 radiation)

The third reaction step (B) gives XRD diffractograms equivalent to those associated with the order–disorder transformation in mechanism 1, ending up with an amorphous sample. Finally, crystalline V_3O_7 is formed exothermally according to reaction (2) above. Mechanism 2 was also found in a parallel experiment performed at 0.7 °C min^{-1} but at much lower temperatures. This temperature effect is observed for both reaction routes (see Table 1), and for equivalent reaction steps in the two different mechanisms. $V_3O_7 \cdot H_2O$ starts to form at 185 °C for 0.7 °C min^{-1} (mechanism 2) and

at 240 °C for 10 °C min^{-1} (mechanism 1), respectively; the reaction takes place close to equilibrium at the lower heating rate.

Somewhat different results are obtained from the DSC experiment at 10 °C min^{-1} with an open crucible, where the gases formed can quickly leave the solid phases and push reactions (1)–(4) to the right. The reactions therefore occur at lower temperatures compared with the 10 hole, 10 °C min^{-1} case. The temperatures for the various reaction steps are higher than for the 0.7 °C min^{-1}, one-hole series. However, the final product is a mixture of *ca.* 50% V_3O_7 (formed according to mechanism 2 above) and *ca.* 50% V_2O_5. Already at 233 °C, small XRD peaks could be seen for crystalline V_2O_5 in an amorphous background. This indicates that two parallel reactions occur prior to the third reaction step (B). The formation of V_2O_5 can originate from a compound containing V^{5+}. Two possible reactions are:

$$2NH_4VO_3 \rightarrow V_2O_5 + 2NH_3 + H_2O \quad (5)$$

$$2NH_4V_3O_8 \cdot \tfrac{1}{2}H_2O \rightarrow 3V_2O_5 + 2NH_3 + 2H_2O \quad (6)$$

V_2O_5 may also be formed, however, from amorphous intermediate states involving V^{5+}. The decomposition into V_2O_5 is endothermic, which may explain why all endothermic peaks are larger and exothermic peaks smaller than in the 10 hole, 10 °C min^{-1} case. Reaction (5) above was also confirmed by heating NH_4VO_3 in air to produce single-phase V_2O_5.

Mechanism 3

An even more complicated reaction route is found using a slow heating rate (0.5 °C min^{-1}) and sealed aluminium crucibles. The DSC curve [Fig. 1(*c*)] exhibits a dominant endothermic chemical reaction (A1). The X-ray diffractograms reveal the initial formation of $V_3O_7 \cdot H_2O$, and mass spectrometry shows the presence of NH_3 and H_2O. The crystalline $V_3O_7 \cdot H_2O$ then undergoes local structural rearrangements, and subsequent rapid decomposition into an amorphous phase (D). The behaviour of the different peaks shows this decomposition to be quite different from that of the two mechanisms discussed above. Mass spectrometry also shows that the two intermediate states, B (mechanisms 1 and 2) and D (mechanism 3) are different. A pronounced N_2 peak just after the A1 reaction step in the mass spectrum is evident, which indicates that the reduction of the vanadium (from mean oxidation state +5 to $+4\frac{1}{3}$) has already started here. Some N_2 and H_2O are liberated at E; the powder undergoes a colour change from brown to blue–black, and XRD shows the formation of single-phase V_6O_{13} (Fig. 5).

An interesting parallel experiment in two steps was performed to show that the same A1 reaction takes place in both mechanisms 1 and 3. NH_4VO_3 in an aluminium crucible with one hole in the lid was first heated at 10 °C min^{-1} from 50 to 270 °C [Fig. 1(*a*)]. After quenching to room temperature, the sample was placed in a sealed crucible and heated to 500 °C. The final compound contained only single-phase V_6O_{13}.

Concluding Remarks

The formation of three vanadium oxide phases from NH_4VO_3 has been observed: V_2O_5, V_3O_7 and V_6O_{13}. The overall reactions are:

$$18NH_4VO_3 \rightarrow 9V_2O_5 + 18NH_3 + 9H_2O \quad (7)$$

$$18NH_4VO_3 \rightarrow 6V_3O_7 + 16NH_3 + 12H_2O + N_2 \quad (8)$$

$$18NH_4VO_3 \rightarrow 3V_6O_{13} + 14NH_3 + 15H_2O + 2N_2 \quad (9)$$

It is clear that VO_x-phase formation is strongly dependent on both the heating rate and the atmosphere surrounding the sample. Furthermore, the lower the final oxidation state, the more critical are the experimental conditions. Armed with a knowledge of the conditions of formation (described above), single-phase V_6O_{13}, V_3O_7 and V_2O_5 and/or mixtures thereof can be obtained consistently.

This work was supported by grants from DARPA [administered through The United States Office of Naval Research (ONR)], The Swedish Natural Research Council (NFR) and The Swedish Board for Technical Development (NUTEK) within the EEC (Joule II) Programme for Non-Nuclear Energy Sources. We also thank Dr. Kjell Jansson of the Arrhenius Laboratory of Stockholm University for his generous assistance with the mass spectrometry studies.

References

1 C. Lampe-Önnerud, T. Gustafsson and J. O. Thomas, *Mater. Res. Soc. Symp. Proc., Solid State Ionics III*, 1993, **293**, 49.
2 F. Theobald, R. Cabala and J. Bernard, *C.R. Acad. Sci. Paris, C*, 1969, **296**, 000.
3 J. Trau, *J. Therm. Anal.*, 1974, **6**, 355.
4 I. K. Bhatnagar, D. K. Chakrabarty and A. B. Biswas, *Ind. J. Chem.*, 1972, **10**, 1025.
5 M. E. Brown, L. Glasser and B. V. Stewart, *J. Therm. Anal.*, 1974, **6**, 529.
6 R. Dziembaj and J. Podolski, *Bull. Acad. Pol. Sci.*, 1978, **26**, 715.
7 S. A. Selim, Ch. A. Philip and R. Ch. Mikhail, *Thermochim. Acta*, 1980, **36**, 287.
8 M. H. Askar, B. S. Girgis and M. A. Khilla, *J. Therm. Anal.*, 1989, **35**, 1315.
9 U. von Sacken and J. R. Dahn, *J. Power Sources*, 1989, **26**, 461.
10 D. A. Skoog and D. M. West, *Fundamentals in Analytical Chemistry*, CBS College Publishing, Hong Kong, 1986, p. 745.
11 F. Theobald and R. Cabala, *C.R. Acad. Sci. Paris*, 1970, **270**, 2138.
12 K. Waltersson, B. Forslund and K-A. Wilhelmi, *Acta Crystallogr., Sect. B*, 1974, **30**, 2644.
13 K-A. Wilhelmi, K. Waltersson and L. Kihlborg, *Acta Chem. Scand.*, 1971, **25**, 2675.
14 E. Andrukaitis, P. Jacobs and J. Lorimer, *Solid State Ionics*, 1988, **27**, 19.
15 R. Enjalbert and J. Galy, *Acta Crystallogr., Sect. C*, 1986, **42**, 1467.
16 C. Lampe-Önnerud and J. O. Thomas, *Eur. J. Sol. State Inorg. Chem.*, accepted.

Paper 4/07607I; *Received* 13*th December*, 1994